INSTABILITIES IN LOW PRESSURE INDUCTIVE DISCHARGES WITH ATTACHING GASES

by

M. A. Lieberman, A. J. Lichtenberg and
A. M. Marakhtanov

Memorandum No. UCB/ERL M99/30

3 June 1999

INSTABILITIES IN LOW PRESSURE INDUCTIVE DISCHARGES WITH ATTACHING GASES

by

M. A. Lieberman, A. J. Lichtenberg and A. M. Marakhtanov

Memorandum No. UCB/ERL M99/30

3 June 1999

ELECTRONICS RESEARCH LABORATORY

College of Engineering
University of California, Berkeley
94720

INSTABILITIES IN LOW PRESSURE INDUCTIVE DISCHARGES WITH ATTACHING GASES

M.A. Lieberman, A.J. Lichtenberg, and A.M. Marakhtanov

Department of Electrical Engineering and Computer Sciences
University of California, Berkeley, CA 94720

ABSTRACT

Plasma instabilities at frequencies 1 Hz–900 kHz have been observed in low pressure inductive processing discharges with attaching gases. Instability windows in pressure and driving power are found. A volume-averaged (global) model of the instability is developed, considering idealized inductive and capacitive energy deposition. As pressure or power are varied to cross a threshold, the instability is born at a Hopf bifurcation, with relaxation oscillations between inductive and capacitive modes causing modulations of charged particle densities, electron temperature, and plasma potential. The oscillations can be so strong that the potential collapses and negative ions flow to the walls.

Submitted to *Applied Physics Letters*
June 3, 1999

Although instabilities in nonmagnetized, attaching gas plasmas at high pressures ($\gtrsim$ 1 Torr) have been well studied in dc glows[1–3] and capacitive discharges[4], there has been only one study reported[5] for low pressure ($\lesssim$ 20 mTorr) inductive discharges of the type increasingly used in plasma-assisted microfabrication technology. Planar or cylindrical coils in a low aspect ratio (length/diameter) discharge are generally used. In the planar configuration used in our experiments, a flat helical coil is wound from near the axis to near the outer radius at one end of a 29.8 cm diameter, 7.62 cm long discharge chamber. The applied power at 13.56 MHz is 100-1000 W with a plasma density in the range 10^{10}–10^{12} cm^{-3}. Because the coil voltage can be as large as several kilovolts, a discharge can also be capacitively driven at low densities (low powers), with a transition to an inductive discharge at high densities (high powers).[6–7]

In a previous experiment[5], instabilities were found with a cylindrical coil using O_2 and Ar/SF_6 (85%Ar, 15% SF_6) gas feeds. The source was a 12 turn copper coil 30 cm in diameter powered by an 0.46 MHz rf generator operated between 200 and 500 watts. With pressures in the range 0.25–10 mTorr, instabilities were observed with frequencies in the range of 1 to 40 kHz. Typically, with increasing pressure the instability grows and then decays, with peak relaxation current modulations on an unbiased Langmuir probe of 50%.

In preliminary experiments, using the planar coil configuration described above, we have also observed oscillations in O_2 and in Ar/SF_6 mixtures. The instabilities were observed on the current to an unbiased Langmuir probe in the center of the discharge and as the optical emission detected by a photomultiplier tube viewing a midplane diameter. The instabilities appeared within power and pressure windows (*e.g.*, 320–600 W at 5.8 mTorr; 4–8 mTorr at 360 W in SF_6) and exhibited a wider range of frequencies (1 Hz–900 kHz) than in the experiments with the cylindrical coil. Relaxation oscillations were sometimes observed having essentially 100% modulation; *i.e.*, the electrons were almost completely expelled during the oscillation. Figure 1 gives one example of an oscillation near 1 kHz

at 540 W in a 5.8 mTorr SF_6 discharge. The optical emission versus time shown in (a) consists of a series of sharp pulses. The corresponding frequency spectrum of the probe current shown in (b) indicates the strongly anharmonic nature of the oscillations. Similar phenomena are seen in Ar/SF_6 mixtures and in O_2 discharges.

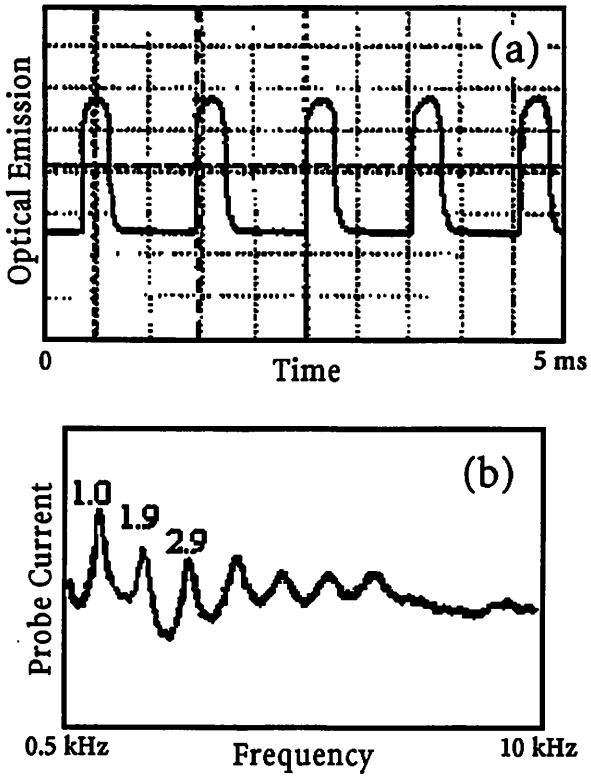

Figure 1. (a) Time-variation of optical emission and (b) frequency spectrum of probe current (b) for a 540 W, 5.8 mTorr SF_6 inductive discharge; the fundamental, second, and third harmonics in kHz are identified in (b).

We have developed a model for the instability for a volume-averaged (global) cylindrical discharge (radius R, length l). We consider electrons (density n_e, temperature T_e), negative ions (density n_-, temperature T_i) and positive ions (density n_+, temperature T_i). We take T_i = const and $T_e \gg T_i$; temperatures are given in equivalent voltage units. The densities are assumed to be uniform within the bulk plasma, dropping sharply at the plasma-sheath edge near the end and circumferential walls. The particle balance equations

are

$$dn_e/dt = K_{\rm iz} n_e n_g - K_{\rm att} n_e n_g - \Gamma_e A_{\rm eff}/V, \tag{1}$$

$$dn_-/dt = K_{\rm att} n_e n_g - K_{\rm rec} n_+ n_- - \Gamma_- A_{\rm eff}/V, \tag{2}$$

where $K_{\rm iz} = K_{\rm iz0}\, {\rm e}^{-\mathcal{E}_{\rm iz}/{\rm T}_e}$ and $K_{\rm att} = K_{\rm att0}\, {\rm e}^{-\mathcal{E}_{\rm att}/{\rm T}_e}$ are Arrhenius forms for the ionization and attachment rate constants, n_g is the neutral gas density, Γ_e and Γ_- are the electron and negative ion fluxes to the walls, and $V = \pi R^2 l$ is the plasma volume. The effective loss area is[9]

$$A_{\rm eff} = 2\pi R^2 h_l + 2\pi R l h_R, \tag{3}$$

where the ratios h_l and h_R of edge-to-center densities are taken from low pressure diffusion theory to be

$$h_l = 0.86/\left(3 + l/2\lambda_i\right)^{-1/2}, \qquad h_R = 0.8/\left(4 + R/\lambda_i\right)^{-1/2}, \tag{4}$$

with λ_i the ion-neutral mean free path. The fluxes are functions of the plasma potential Φ (with respect to the walls) through the Boltzmann relations

$$\Gamma_e = \tfrac{1}{4} n_e \bar{v}_e\, {\rm e}^{-\Phi/{\rm T}_e}, \qquad \Gamma_- = \tfrac{1}{4} n_- \bar{v}_-\, {\rm e}^{-\Phi/{\rm T}_i}, \tag{5}$$

where $\bar{v}_e = (8e{\rm T}_e/\pi m)^{1/2}$ and $\bar{v}_- = (8e{\rm T}_i/\pi M_-)^{1/2}$ are the electron and negative ion mean speeds. A simplified model[10] is used for the positive ion flux appropriate to a low pressure diffusion equilibrium,

$$\Gamma_+ = n_e u_B + \tfrac{1}{4} n_- \bar{v}_-, \tag{6}$$

where $u_B = (e{\rm T}_e/M_+)^{1/2}$ is the Bohm (ion sound) velocity. The conditions of quasi-neutrality in the bulk plasma, $n_+ = n_e + n_-$, and at the walls, $\Gamma_+ = \Gamma_e + \Gamma_-$ are assumed.

The energy balance equation is

$$\frac{d}{dt}\left(\frac{3}{2} n_e {\rm T}_e\right) = P_{\rm abs} - P_{\rm loss}, \tag{7}$$

where

$$P_{\rm loss} = K_{\rm iz} n_e n_g \mathcal{E}_{\rm iz} + K_{\rm att} n_e n_g \mathcal{E}_{\rm att} + \Gamma_e \left(\Phi + 2\,{\rm T}_e\right) A_{\rm eff}/V + \Gamma_- \Phi A_{\rm eff}/V \tag{8}$$

is the energy loss per unit volume. The surface terms in (8), proportional to Φ, give the energy losses for positive ions that fall across the sheath potential, and the term proportional to $2\,T_e$ gives the electron kinetic energy carried to the walls; the negative ion flux to the walls yields a negligible energy loss because $T_i \ll T_e$.

In (7), $P_{abs} = P_{ind} + P_{cap}$ is the power absorbed per unit volume. Inductive power is transferred to electrons within a skin layer of thickness δ near the coil-plasma surface. For a fixed coil current I_{rf}, the power transfer depends on n_e and is low at low densities, where the weakly conducting plasma loop acts as an open circuit, and is low at high densities, where the highly conducting loop acts as a short circuit,[11]

$$P_{ind} = I_{rf}^2 R_{ind} \frac{n_e n_0}{n_e^2 + n_0^2} \frac{1}{V}, \tag{9}$$

where R_{ind} depends on the power deposition volume, and n_0 gives the density for maximum power; *i.e.*, where $\delta \sim V/A_{eff}$.

Electron heating is also produced by capacitive coupling of the coil voltage across the dielectric window to the plasma. The voltage is divided across the window and sheath capacitances. Since the sheath capacitance scales for high sheath voltages as n_e, we obtain[11]

$$P_{cap} = I_{rf}^2 R_{cap} \frac{n_c}{n_e + n_c} \frac{1}{V}, \tag{10}$$

where R_{cap} depends on the degree of capacitive coupling to the plasma (window thickness), and n_c specifies the capacitance at low voltages.

Differential equations (1), (2) and (7) can be integrated, together with the subsidiary conditions, to produce the dynamical behavior. The basic dynamics leading to relaxation oscillation behavior are: (1) the discharge reaches a quasi-equilibrium electron density in inductive mode at low negative ion density; (2) the negative ion density builds up slowly, leading to loss of the quasi-equilibrium; (3) electrons are lost rapidly and the discharge decays to a capacitive state; (4) negative ions decay slowly until the discharge can re-establish the inductive mode. In Fig. 2, results of the time integrations are given for n_e, n_-, T_e, Φ and Γ_- for a typical case with SF_6 parameters and a ratio of peak capacitive/peak inductive power $2R_{cap}/R_{ind}$ of 2%. The electron density oscillation is similar to the optical

emission oscillation in Fig. 1, and the modulation is so deep that the potential collapses and negative ions escape to the walls.

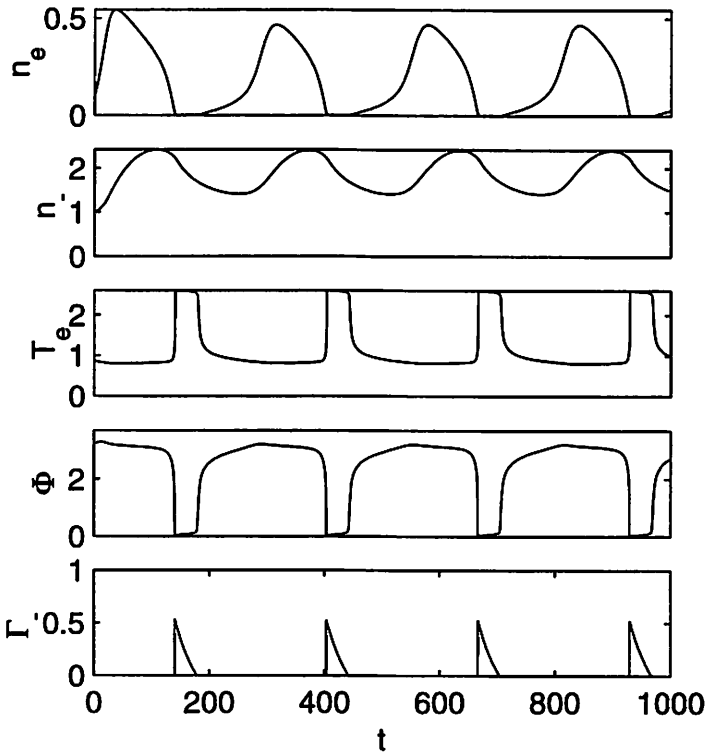

Figure 2. Global model time variation of n_e (units of 10^{10} cm^{-3}); n_- (units of 10^{10} cm^{-3}); T_e (units of eV); Φ (units of V), and $\Gamma_- \propto n_- e^{-\Phi/T_i}$ (units of 10^{10} cm^{-3}) for a 6 mTorr SF_6 discharge with $2R_{cap}/R_{ind}$ equal to 2% (time is in units of 10 μs).

To understand the physics, we obtain a reduced set of equations by noting that, typically, there are three time scales. The fastest time scale is for changes in power (7), the next fastest is for changes in electron density (1), and the slowest is for changes in negative ion density (2). Using this ordering, we first set $d(\frac{3}{2}n_e T_e)/dt = 0$ to eliminate the highly temperature sensitive term K_{iz} in (7) to obtain

$$(K_{iz} - K_{att})n_e n_g \mathcal{E}_{iz} = P_{abs} - K_{att} n_e n_g \mathcal{E}_{iz} - K_{att} n_e n_g \mathcal{E}_{att} - [\Gamma_e(\Phi + 2T_e) + \Gamma_- \Phi] A_{eff}/V. \tag{11}$$

Substituting (11) into (1), we find

$$\mathcal{E}_{\rm iz}\frac{dn_e}{dt} = P_{\rm abs} - K_{\rm att}n_e n_g(\mathcal{E}_{\rm iz} + \mathcal{E}_{\rm att}) - [\Gamma_e(\Phi + 2\,\mathrm{T}_e + \mathcal{E}_{\rm iz}) + \Gamma_-\Phi]\,A_{\rm eff}/V. \qquad (12)$$

Setting $dn_e/dt = 0$ in (12) yields an equation for $n_-(n_e)$, where T_e and Φ are obtained from (11) and quasi-neutrality. The results (dashed lines) in the n_- versus n_e phase plane are shown for two different cases in Fig. 3; dn_-/dn_e is positive "below" these lines. The abrupt increase in the quasi-equilibrium n_- density from (12) at a small value of n_e is due to the collapse of the plasma potential, where the loss of electrons can no longer match the positive ion loss, so that negative ions must also escape to preserve the charge equilibrium. On the same figure we also plot (dot-dashed lines) the equation for $n_-(n_e)$ obtained by setting $dn_-/dt = 0$ from (2); dn_-/dn_e is positive "below" these lines.The crossing of the two $n_-(n_e)$ curves obtained from (12) and (2) gives the equilibrium.

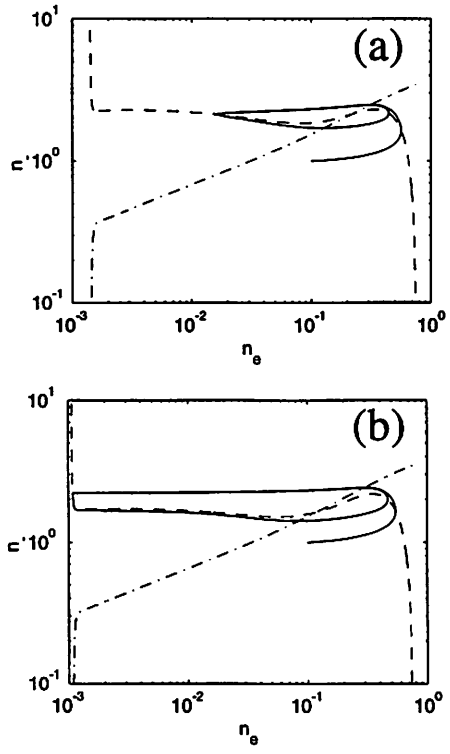

Figure 3. Global model n_- versus n_e phase plane for a 6 mTorr SF_6 discharge with $2R_{\rm cap}/R_{\rm ind}$ equal to (a) 4% and (b) 2%; the dashed line gives $dn_e/dt = 0$, the dot-dashed line gives $dn_-/dt = 0$, and the solid curve gives the numerical integration of the equations of motion; case (b) corresponds to the time variation shown in Fig. 2.

Examining a small departure from the equilibrium will easily convince the reader that the equilibrium is unstable if both slopes dn_-/dn_e are positive at the crossing, with the slope from (2) steeper than the slope from (12). All other crossings are stable. We have chosen the coil current $I_{\rm rf}$ in Fig. 3 to illustrate (a) the instability onset shortly after the Hopf bifurcation[12] (4% capacitive/inductive power ratio) and (b) a strong oscillation between inductive and capacitive modes with collapse of the potential (2% capacitive/inductive power ratio). Superimposed on these figures are the actual trajectories in the phase plane, for which the complete time-dependent equations are solved with no ordering. In Fig. 3(a) the oscillations are weakly modulated. In Fig. 3(b), corresponding to the time variations in Fig. 2, fully developed relaxation oscillations are seen similar to those observed in our planar coil experiment.

According to our model, below 5 mTorr in SF_6 the potential no longer collapses as n_e decays. In this case a relaxation oscillation can still occur between a low n_e near-extinguished state and a high n_e inductive state; re-ignition from the low n_e state occurs when n_- decays to a sufficiently low value that electropositive ignition occurs.

In conclusion, we have shown that low pressure inductive discharges with attaching gases are subject to instabilities if the parameters lie within a certain range. Such relaxation oscillations have been observed both with a cylindrical coil using 0.46 MHz driving power and with a planar coil using 13.56 MHz driving power in our experiments.

The authors acknowledge the support provided by NSF Grant ECS-9820836, the Lam Research Corporation, California Industries, and the State of California UC-SMART Program under Contract 97-01.

REFERENCES

1. R.A. Hass, *Phys. Rev. A* **8** 1017 (1973).

2. W.L. Nighan and W.J. Wiegand, *Phys. Rev. A* **10** 922 (1974).

3. A.D. Barkalov and G.G. Gladush, *Sov. Phys. Tech. Phys.* **24** 1203 (1979).

4. E. Metsi, E. Gogolides, and A. Boudouvis, *Phys. Rev. E* **54** 782 (1996).

5. M. Tuszewski, *J. Appl. Phys.* **79** 8967 (1996).

6. I.M. El-Fayoumi, I.R. Jones, and M.M. Turner, *J. Phys. D: Appl. Phys.* **31** 3082 (1998).

7. M.A. Lieberman and R.W. Boswell, *J. Phys. IV France* **8** Pr7-145 (1998).

9. M.A. Lieberman and A.J. Lichtenberg, *Principles of Plasma Discharges and Materials Processing,* (Wiley, New York, 1994) Chap. 5, pp. 137–140.

10. I.G. Kouznetsov, A.J. Lichtenberg, and M.A. Lieberman, *Plasma Sources Sci. Technol.* **5** 662 (1996).

11. M.A. Lieberman and A.J. Lichtenberg, *Principles of Plasma Discharges and Materials Processing,* (Wiley, New York, 1994) Chap. 12, pp. 388–399.

12. A.J. Lichtenberg and M.A. Lieberman, *Regular and Chaotic Dynamics,* (2nd ed., Springer, New York, 1992) Chap. 7, pp. 461–468.